fire

MDPI

Article

Chitosan Oligosaccharide@Melamine Polyphosphate Modified Polylactic Acid with Enhanced Flame Retardancy

Mei Zhao [1,*], Guoqiang Dong [1], Xu Lu [1], Yajie Zhao [1], Jingjing Gao [1], Xinxin Wei [1], Chenhui Xu [1], Yu Liu [1], Lianqiang Li [1] and Yachao Wang [2,*]

[1] Institute for Hygiene of Ordnance Industry, Xi'an 710065, China
[2] School of Resources Engineering, Xi'an University of Architecture and Technology, Xi'an 710055, China
* Correspondence: zm@xauat.edu.cn (M.Z.); wangyachao@xauat.edu.cn (Y.W.)

Abstract

A novel material, chitosan oligosaccharide@melamine polyphosphate (CMP), with enhanced flame-retardant and hydrophobic properties, was synthesized by cross-linking melamine polyphosphate (MPP) with chitosan oligosaccharide. Compared with MPP, the CMP overcomes its inherent drawbacks when used as a flame retardant in polylactic acid (PLA) composites, namely the high loading demand and unsatisfactory interfacial compatibility with the polymer matrix. The results demonstrated that the peak heat release rate (p-HRR) dropped significantly in comparison to pure PLA, from 304.69 $kW \cdot m^{-2}$ to 210.39 $kW \cdot m^{-2}$, while the fire performance index (FPI) increased from 0.1 to 0.48 $s \cdot m^{-2} \cdot kW^{-1}$. Furthermore, the fire growth index (FGI) decreased from 1.51 $kW \cdot m^{-2} \cdot s^{-1}$ to 1.03 $kW \cdot m^{-2} \cdot s^{-1}$. Additionally, the CMP demonstrated enhanced thermal stability, making the pyrolysis activation energy E_α increase from 135.04 to 191.97 kJ/mol during 308~416 °C by pyrolysis kinetics. Compared to composite PLA incorporating pristine MPP, the CMP-modified counterpart exhibits superior mechanical properties and significantly enhanced hydrophobicity, evidenced by a maximum water contact angle reaching 93.96°. It provides a strategy for adapting phosphorus-based flame retardants for PLA, thereby broadening their applicability across diverse scenarios.

Keywords: polylactic acid; melamine polyphosphate; chitosan oligosaccharide; flame retardant

1. Introduction

With the dwindling of petroleum reserves and rising attention to environmental conservation, biodegradable thermoplastics sourced from natural renewable resources have witnessed a rapid expansion in both academic research and industrial applications [1]. Extensive research highlights that polylactic acid (PLA), owing to its excellent mechanical and plastic properties, has garnered increasing attention and application across diverse sectors such as 3D printing, textiles, and medicine [2,3]. However, enhancing flame retardancy of PLA is critically important, as its inherently low thermal stability and propensity for violent molten dripping during combustion substantially limit its adoption in demanding fields like the electronics and automotive industries [4,5].

Melamine polyphosphate (MPP) is recognized as a high-efficiency, halogen-free flame retardant, primarily based on nitrogen and phosphorus [6]. MPP possesses bifunctional properties in intumescent flame-retardant systems: it not only acts as the acid source but also serves as the precursor of the gas source that drives char layer expansion. During thermal decomposition, the polyphosphoric acid generated from MPP plays a vital role

Check for updates

Academic Editor: Siqi Huo

Received: 25 May 2026
Revised: 26 June 2026
Accepted: 26 June 2026
Published: 1 July 2026

Copyright: © 2026 by the authors. Licensee MDPI, Basel, Switzerland. This article is an open access article distributed under the terms and conditions of the Creative Commons Attribution (CC BY) license.

in catalyzing charring of the PLA matrix [7]. Furthermore, MPP exhibits low environmental persistence, negligible bioaccumulation, and is thus considered environmentally benign [8]. Its efficacy as a flame retardant has been well-documented in previous research. Decsov et al. [9] adopted a carbon dioxide-assisted batch foaming process, added aluminum tris(diethylphosphinate) and MPP to synthesize flame-retardant foams, which achieved a LOI of 25.0%, delayed ignition, and reduced the pHRR by 23%. Nevertheless, a significant challenge associated with MPP, as a representative phosphorus-based flame retardant, is its tendency to require substantial addition amounts and exhibit poor compatibility with the host matrix when incorporated into PLA [10]. These factors frequently lead to substantial degradation of mechanical properties of PLA, thereby impeding its widely practical applications [11].

To enhance MPP's compatibility when incorporated into polymer matrices as a flame retardant, modification with bio-based materials presents an effective strategy [12]. Chitosan oligosaccharide (COS) is a green, bio-based material derived from chitosan (CS) via enzymatic or chemical hydrolysis [13]. Previous investigations have demonstrated chitosan's efficacy in improving the compatibility of phosphorus-based flame retardants, while simultaneously functioning as a bio-based carbon source to impart synergistic flame retardancy [14]. In contrast to CS, COS, with its shorter chain length and accessible free amino groups, exhibits superior water solubility and enhanced chemical reactivity [15], which facilitates convenient production and processing. Xu et al. [16] synthesized a novel flame retardant, characterized by multiple hydroxyl groups, by reacting COS with ammonium polyphosphate (APP) and ammonium octamolybdate. Zhang et al. [17] completely inhibited the PET melt droplet formation by using COS and guanidinium urea phosphate. It not only preserved the mechanical integrity of polyurethane but also delivered an enhanced flame retardancy [16]. Despite these promising aspects, exploring the application of COS in flame retardants remains relatively nascent.

This work holds several distinct innovations. Firstly, a novel eco-friendly PLA composite was prepared with excellent flame retardancy and hydrophobicity using a facile process. Secondly, a new composite flame-retardant CMP was synthesized by grafting COS onto MPP. The introduction of COS effectively improves the compatibility between MPP and PLA, and the as-formed C-N-P synergistic system greatly boosts its flame retardancy. Thirdly, comprehensive characterizations were carried out to reveal the underlying flame-retardant mechanisms of PLA/CMP composites. Overall, this study provides an effective strategy for optimizing phosphorus-based flame retardants.

2. Materials and Methods

2.1. Materials

All reagents were used directly without further purification. COS (powder, molecular weight no greater than 2000) was acquired from Shanghai Macklin Biochemical Co., Ltd. (Shanghai, China). PLA with a density of 1.24 g/cm^3 was offered by NatureWorks of the United States (Plymouth, MN, USA). Flake NaOH (purity > 97%) was procured from Shanghai Aladdin Biochemical Technology Co., Ltd. (Shanghai, China). Anhydrous ethanol with a purity higher than 99.7% came from Greagent, an affiliated brand of Shanghai Titan Scientific Co., Ltd. (Shanghai, China). MPP was manufactured by Guangzhou Boxin Fine Chemical Co., Ltd. (Guangzhou, China).

2.2. Preparation of Samples

2.2.1. Preparation of CMP

Firstly, the 18 g MPP was gradually introduced into 350 mL deionized water to initiate the preparation process under mechanical stirring at 750 rpm. The resulting suspension

was maintained at 70 °C with continuous mechanical agitation (750 rpm) for 10 min to ensure homogeneous dispersion. Concurrently, 12 g of COS was dissolved in 300 mL of ethyl ethanol under constant stirring (350 rpm) at 35 °C for 5 min, followed by pH adjustment to 9.0 using 5 mol/L NaOH solution. The COS–ethanol solution was then introduced dropwise into the MPP suspension through continuous mechanical mixing at 80 °C (1000 rpm) for another 30 min. Subsequent to the reaction, the mixture was allowed to stand undisturbed for 2 h to facilitate complete interaction, yielding the MPP@COS composite solution. The product CMP was obtained by repeated filtration and dried for 48 h.

2.2.2. Preparation of the Samples

The dried 93 g PLA and 7 g additives were pre-mixed. After the mixing is completed, it is added to the double helix melt blending machine for melt blending. Melt compounding was carried out using a laboratory twin-screw extruder with a gradient temperature setting along the barrel. Temperatures of zones I to VI were controlled at 120 °C, 135 °C, 160 °C, 180 °C, 190 °C and 195 °C, respectively. Other fixed processing parameters included an extrusion pressure of 3.6 bar, a feeding rate of 18.0 rpm and a screw rotation speed of 38.0 rpm. The extruded PLA thread is cut into pellets after cooling and dried for later use. The dried PLA particles were pressed into the required sample specifications by an electric tableting machine. The formula of each group of samples in the experiment is shown in Table 1, and the preparation flow chart is shown in Figure 1.

Table 1. The formulation of PLA sample.

Samples	PLA (g)	CMP (g)	MPP (g)	COS (g)
S0	100	-	-	
S1	93	-	-	7
S2	93	-	7	-
S3	93	7	-	-

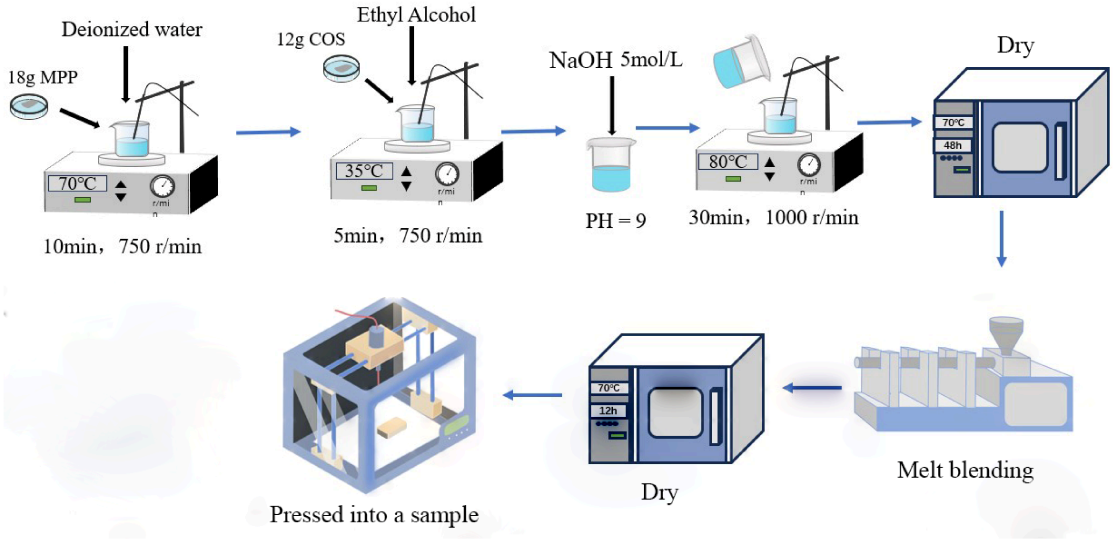


Figure 1. Schematic diagram of PLA-CMP preparation.

2.3. Characterizations

The functional groups and the structural composition were analyzed by attenuated total reflection Fourier transform infrared spectra (ATR-FTIR) data using the Thermo Scientific iS50 (Thermo, Singapore) infrared spectrometer. The samples were prepared

at room temperature using the KBr pellet method, and 32 test scans were performed in an infrared spectrophotometer with wave numbers ranging from 500 to 4000 cm^{-1}. A Mettler-Toledo analyzer (TGA/DSC3 IST16, Mettler-Toledo Company, Columbus, OH, USA) was used to perform thermogravimetric/micro-thermogravimetric (TG/DTG) testing on composite PLA. The results of weight loss were further adopted to analyze the pyrolysis kinetic behavior. Under a pure N_2 atmosphere, the weight loss of samples was recorded during 30~1000 °C with a 20 °C/min heating. The tensile properties of the samples were evaluated using a tensile tester (FR-108C) at room temperature. Samples with dimensions of 100 mm × 30 mm × 3 mm were subjected to tensile testing at a crosshead speed of 5 mm/min. The wettability of water on the surface of the samples was quantified using a static water contact angle (WCA) meter (JCY-3, Farrer, Shanghai, China). The WCA images were obtained and calculated by a tangent algorithm. The mean WCA value was determined from measurements at five additional positions, with a measurement tolerance of 2°.

The results of fire spread were tested by the ZY6423-I cone calorimeter (CC, Zhongnuo Instrument Co., Ltd., Jinan, China) on a sample of 100 × 100 × 5 mm^3 by ISO 5660-1:2015 (Amd 1:2019) [18]. Before testing, the samples were adjusted to an equilibrium condition of 75% relative humidity and 28 °C. The 100 × 100 × 5 mm^3 samples were placed horizontally on a load cell 35 mm away from the cone heater. All test specimens were positioned in a horizontal orientation and subjected to a uniform external heat flow of 35 $kJ \cdot m^{-2}$. The combustion behavior of the samples was assessed through real-time monitoring of heat release rate (HRR), peak HRR (pHRR), ignition time (TTI), time to pHRR (Tp), total heat release (THR), and weight loss (WL). Fire safety was evaluated using the fire performance index (FPI) and fire growth index (FGI) calculated via Formulas (1) and (2). FGI quantifies thermal decomposition resistance, where higher values indicate accelerated fire propagation and increased hazard. FPI characterizes flashover duration, with higher values reflecting slower flame spread and extended evacuation time. Flame retardancy index (FRI, Formula (3)) classified materials as poor (FRI < 1), good (1 < FRI < 10), or excellent (10 < FRI < 100) [19].

The UL-94 vertical burning rating was determined using a vertical burning tester (DX8522, Dongguan Kepin, Dongguan, China) in accordance with ASTM D3801, with sample dimensions of 130 × 13 × 3 mm^3. Meanwhile, the limiting oxygen index (LOI) was tested by a limiting oxygen index tester following the corresponding standard method [20].

$$FPI = TTI/pHRR \tag{1}$$

$$FGI = pHRR/T_p \tag{2}$$

$$FRI = \frac{\left(THR * \frac{pHRR}{TTI}\right)_{Control}}{\left(THR * \frac{pHRR}{TTI}\right)_{Composite}} \tag{3}$$

3. Results and Analysis

3.1. ATR-FTIR Analysis

3.1.1. COS and CMP Infrared Spectroscopic Analyses

As illustrated in Figures 2 and 3, the FTIR spectra of COS and CMP exhibit distinct vibrational absorption characteristics. Remarkably, the broad absorption band centered at 3200 cm^{-1} in the COS spectrum arises from the coupling of vibrational modes between -OH and -NH_2 groups within a hydrogen-bonded network [21]. The peak at 1620 cm^{-1} is attributed to the stretching vibration of -NH_2 [22]. The peak at 2932 cm^{-1} is attributed to the stretching vibration of -CH with -CH_2, while its bending vibration occurs at 1324 cm^{-1} [23].

The peak at 1083 cm^{-1} is assigned to the stretching vibration of C-O-C [22]. Meanwhile, characteristic absorption features at 1620 cm^{-1} and 1379 cm^{-1} are diagnostically assigned to the stretching modes of C=O groups and bending vibrations of C-N bonds [13].

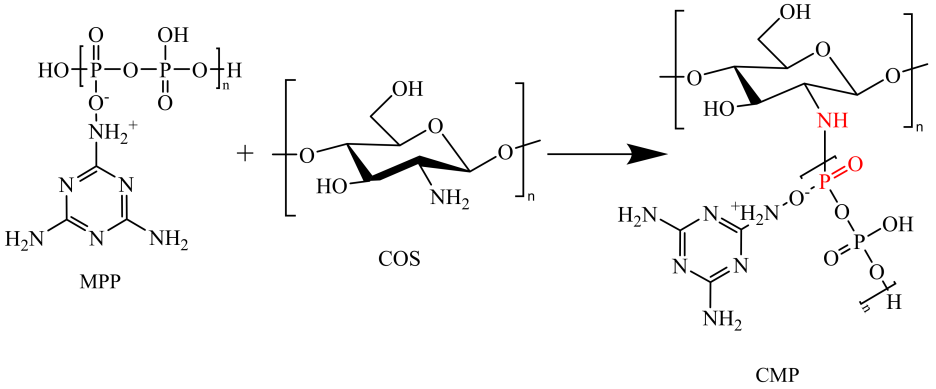


Figure 2. Schematic diagram of chemical reaction.

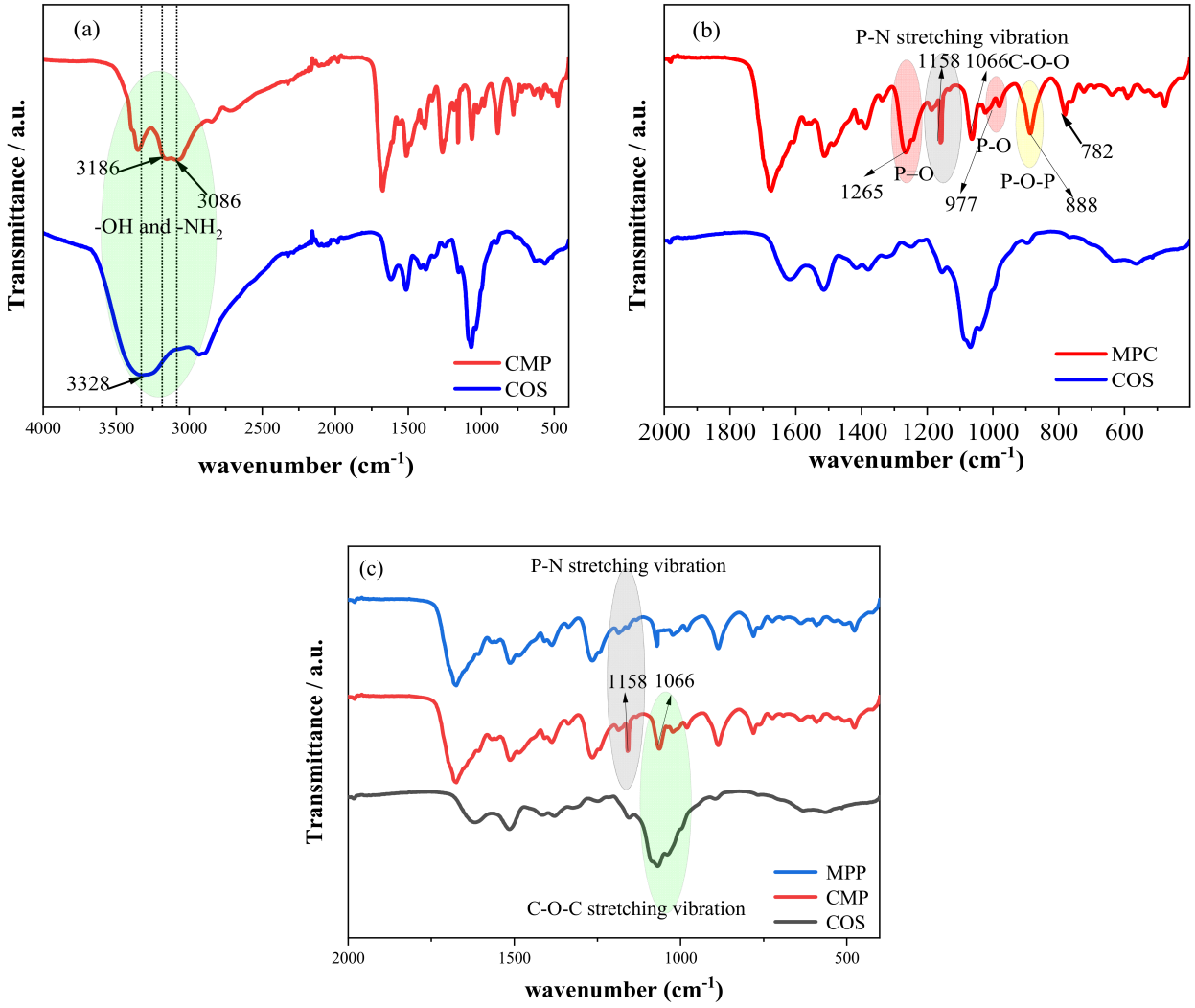


Figure 3. Infrared spectra of COS and CMP (**a**) 4000−500 cm^{-1} range; (**b**) 2000−400 cm^{-1} range; (**c**) spectra of COS, CMP and MPP.

The infrared analysis of CMP reveals critical structural features. For the MPP component, the absorption band located at 1674 cm^{-1} originates from the vibration of C-N bonds

in its pyrimidine ring structure [24]. Newly emerged peaks at 1265 cm^{-1} and 977 cm^{-1} are unambiguously assigned to P=O and P-O stretching vibrations, respectively, while the distinct peak at 886 cm^{-1} arises from the P-O-P bridge stretching vibration [25,26]. Notably, the N-H peak at 1620 cm^{-1} exhibits reduced intensity with a significant wavenumber shift, accompanied by the emergence of a characteristic deformation vibration at 1603 cm^{-1} corresponding to secondary amine (-NH-) groups [27]. As shown in the comparison of Figure 3c, a distinct P-N stretching vibration peak was observed at 1158 cm^{-1}, which directly indicated the presence of phosphoramide groups [28]. The vibrational absorption peak at 1066 cm^{-1} on the C-O-C bond confirms the incorporation of COS. These spectral transformations confirm the covalent conjugation between COS and MPP, wherein the amino groups of COS nucleophilically attack the electrophilic phosphorus atoms generated during MPP hydrolysis, forming stable phosphoramidate linkages (-NH-P=O) [29]. The reaction process is shown in Figure 2.

3.1.2. Infrared Spectral Analysis of Modified PLA

The infrared spectrum of modified PLA is depicted in Figure 4. The CMP exhibits a distinctive peak at 1752 cm^{-1}, corresponding to the formation of C=O [30]. The peak exhibits a significant shift relative to that exhibited by PLA at 1749 cm^{-1}. The carbonyl group could generate stable residues, which serve as barriers during combustion, effectively blocking the flame from sustained combustion, and resulting in a lower HRR and flue gas temperature [31]. The characteristic peak located at 1189 cm^{-1} originates from the stretching vibration of C-O bonds. As for CMP, three distinct absorption peaks appear at 2944 cm^{-1}, 1454 cm^{-1} and 1089 cm^{-1}, which correspond to the asymmetric stretching of C-H bonds, the bending vibration of C-H groups, and the asymmetric stretching of C-O-C bonds, respectively [32].

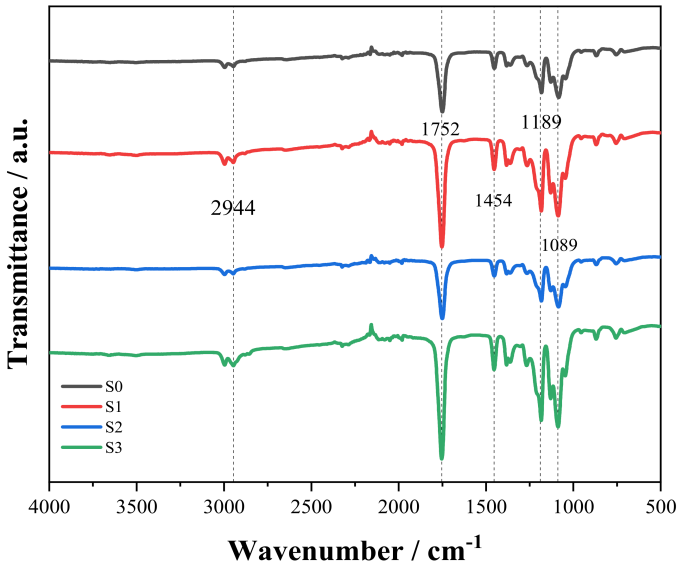


Figure 4. Infrared spectra of modified PLA.

3.2. Flame Retardancy

Figure 5a illustrates the HRR curves of all as-prepared specimens. The S0 begins burning at 60 s and reaches its peak at 404 s, which is 304.69 $kW \cdot m^{-2}$. The doped CMP markedly diminishes the combustion intensity, with the p-HRR of the CMP reaching 210.39 $kW \cdot m^{-2}$ and exhibiting a peak 30.95% lower than that of the S0, due to the formation of dense and resilient residues by CMP, and the released non-flammable gases such as NH_3 and CO_2 [33]. Additionally, the combustion of S2 is divided into two stages. The

first p-HRR corresponds to the temporary protective effect of the residual layer, while the second p-HRR corresponds to the decomposition of the residues under continuous high temperatures. Interestingly, the CMP-containing sample shows a single combustion peak, verifying the superior stability of the residues formed with CMP. In other words, the flame-retardant effect of CMP is clearly due to the cross-linking reaction of MPP with COS, triggering a synergistic flame-retardant effect. Figure 5b demonstrates the average exothermic rate profile of all the samples. The peak average exothermic rate of S0 was 134.38 kW·$(m^2 \cdot s)^{-1}$, and the peak values were reduced by 42.7%, 15.6%, and 60.6% after the addition of COS, MPP, and CMP, respectively. It indicates that the incorporation of CMP is an effective flame-retardant strategy verified by the reduced $HRR_{average}$, heat transfer, and burning intensity.

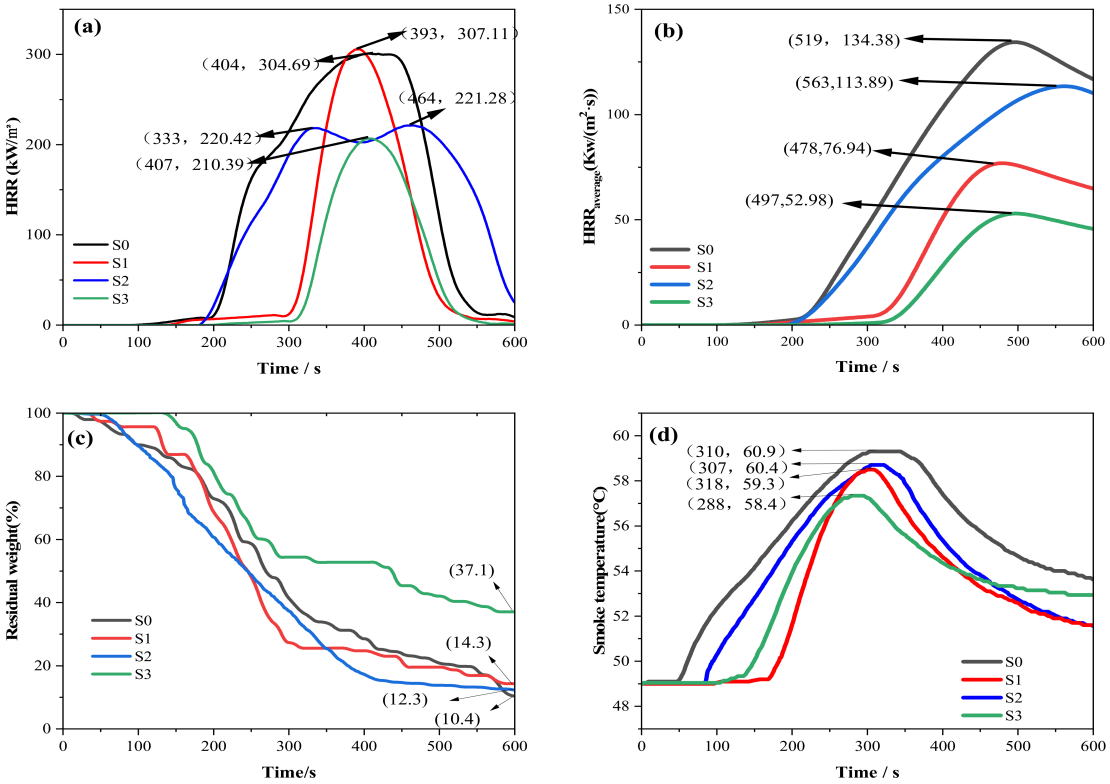


Figure 5. The flame retardancy of samples, including (**a**) HRR, (**b**) $HRR_{average}$, (**c**) residual weight, and (**d**) smoke temperature.

Figure 5c illustrates the weight loss of the sample subject to combustion. It is observed that S0 presents no residues left after combustion, and the addition of COS and MPP alone does not significantly contribute to the reduction of weight loss. However, for CMP, the residual weight increases from 14.3% to 37.1%, indicating a significant synergistic effect of CMP in promoting residual char formation. At 300 s, the curve of CMP has a smooth buffer section. This is due to the formation of a porous residual layer, and as the flame continues to burn, the barrier begins to be destroyed and the mass begins to gradually decrease. In contrast, CMP exhibits a markedly reduced weight loss during combustion, due to the as-formed residues effectively isolating oxygen and heat, thereby presenting enhanced thermal stability. This finding is consistent with the results of the HRR curves.

Asphyxiation is the most common cause of death in a fire and thus, the smoke temperature can be a reliable indicator of the fire safety performance [34]. Figure 5d illustrates the smoke temperature produced by the samples during combustion. The maximum smoke temperature of S0 can reach 60.9 °C, while the peak smoke temperature of CMP is 57 °C,

due to the formation of porous residues during the combustion of PLA following cross-linking reaction modification. On one hand, these char layers effectively mitigate flue gas emission; on the other hand, they impede heat conduction between the combustion zone and the flue gas. This part corresponds to the smoothing period at 300 s in the weight loss curve. In parallel, CMP demonstrates a discernible gas-phase flame-retardant mechanism. The pyrolysis phase yields inert gases that contribute to flue gas dilution and thermal quenching. Additionally, the decomposition of the flame retardant generates phosphorus-centered radicals capable of scavenging reactive species, consequently suppressing the generation of high-temperature flue gases [35].

However, as shown in Table 2, CMP holds the longest time to ignition (TTI) of 202 s. Its higher FPI index (0.48 $kW \cdot m^{-2} \cdot s^{-1}$) and lower FGI (1.03 $s \cdot m^2 \cdot kW^{-1}$) index indicate that it has a lower burning intensity. This implies that it offers a longer evacuation time and enhanced safety in the event of a fire. Furthermore, its elevated FRI index serves to reinforce this assertion.

Table 2. Combustion parameters of samples.

Sample	TTI/s	Tp/s	p-HRR/ $kW \cdot m^{-2}$	FGI/ $kW \cdot m^{-2} \cdot s^{-1}$	FPI/ $(m^2 \cdot s/kW)$	Residues/ %	THR/ $MJ \cdot m^{-2}$	FRI
S0	60 ± 3	404 ± 6	304.69 ± 6.0	1.51 ± 0.05	0.10 ± 0.02	10.40 ± 0.4	70.15 ± 2.1	1.0
S1	158 ± 6	393 ± 7	307.11 ± 8.4	1.56 ± 0.05	0.26 ± 0.01	13.83 ± 0.6	38.94 ± 1.2	4.7
S2	151 ± 6	333 ± 5	220.42 ± 4.9	1.33 ± 0.04	0.34 ± 0.04	12.04 ± 0.5	66.36 ± 2.0	3.8
S3	202 ± 8	407 ± 6	210.39 ± 5.2	1.03 ± 0.05	0.48 ± 0.03	34 ± 1.4	27.41 ± 1.8	12.5

According to the results of the vertical burning test in Table 3, the incorporation of MPP improves the self-extinguishing ability of PLA because phosphorus-based flame retardants enhance the flame retardancy via their inherent properties, including radical scavenging and catalytic charring. In addition, the LOI values of all three experimental groups increased, with the most significant increment observed in S2. It indicates that CMP can effectively enhance the flame retardancy of PLA.

Table 3. UL-94 and LOI test results.

Sample	UL-94				LOI(%)
	t_1/s	t_2/s	Dripping	Rating	
S0	burn out	-	Yes	NR	19.8
S1	burn out	-	Yes	NR	21.2
S2	3.4 ± 0.6	burn out	Yes	V-2	22.7
S3	5.8 ± 0.5	burn out	Yes	V-2	23.8

Note: t_1 and t_2 is flame duration of the first and second ignition, respectively.

3.3. TG Analysis

TG/DTG/DSC analysis is a method that can be employed to effectively analyze the thermal stability [36]. Table 4 summarizes the key thermal decomposition parameters, including the 5% weight loss temperature ($T_{d5\%}$), 30% weight loss temperature ($T_{d30\%}$), initial decomposition temperature (T_i), final decomposition temperature (T_f), and maximum weight loss temperature (T_{max}). The statistical thermal stability index temperature (T_S) can be calculated using Equation (4) [37], and the integral process decomposition temperature can be calculated using Equation (5), where A* is the ratio of the area under the curve to the total area of the rectangle.

$$T_S = 0.49[T_{d5\%} + 0.6(T_{d30\%} - T_{d5\%})] \quad (4)$$

$$IPDT(^{\circ}C) = A^{*}\left(T_f - T_i\right) + T_i \quad (5)$$

Table 4. TG parameters of samples.

Samples	$T_{d5\%}$/°C	$T_{d30\%}$/°C	T_i/°C	T_f/°C	T_{max}/°C	T_S/°C	IPDT/°C
S0	336	365	30	1000	376	173.166	366.978
S1	339	364	30	996	378	173.46	367.4238
S2	332	364	30	994	378	172.088	371.5452
S3	325	360	30	998	375	169.54	372.0264

The T_S and IPDT values can be used to assess the impact of the cross-linking reaction between MPP and COS on thermal stability [38]. In comparison to the thermal stability temperature of S0 (173.166 °C), the thermal stability temperature of CMP decreased to 169.54 °C, while the IPDT value increased. This suggests that the cross-linked structure formed by CMP favors enhancing the thermal stability of PLA.

Figure 6a illustrates the TG curves of the samples. All samples completed their main weight loss during 300–400 °C. After the incorporation of MPP into the PLA matrix, the weight loss temperatures of the composites shifted to lower values, as the flame retardant catalyzed the thermal decomposition of the PLA matrix at relatively lower temperatures. During 400–1000 °C, the formed char layer undergoes further degradation; S0 was almost completely burnt with no residues remaining at 600 °C. In contrast, the residual amount of CMP increased to 3%. The observed increase in residual carbon content suggests that the presence of CMP can facilitate the residual formation, which is indicative of enhanced thermal stability of PLA due to the cross-linking between MPP and COS.

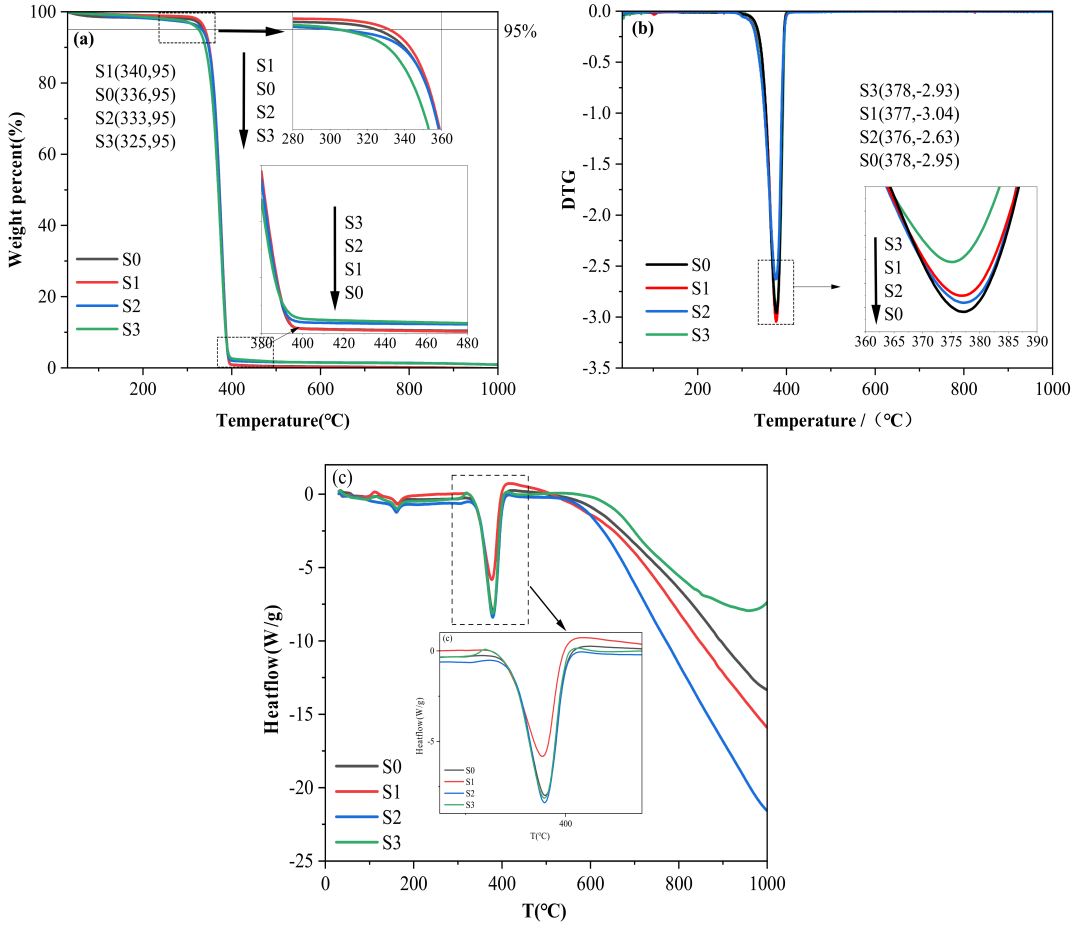


Figure 6. TG/DTG/DSC curves of samples, including (**a**) TG, (**b**) DTG, and (**c**) DSC, respectively.

The DTG curve of the sample is depicted in Figure 6b. At 70 °C, the small molecules undergo volatilization, resulting in a slight slope. The maximum degree of weight loss occurs around 380 °C, corresponding to a rapid weight loss. It can be observed that the value of CMP at this time is significantly lower than the value of S0 over S1, indicating that CMP has a lower decomposition rate. This corresponds to the decomposition of MPP into polyphosphoric acid and ammonia gas, while the expanding residues impede the further decomposition of PLA by blocking the heat exchange. This result also further confirms the higher residual weight of the CMP-containing sample in the TG images than in the other samples.

Figure 6c shows the DSC curve of the sample. The curve exhibits a distinct absorption peak at approximately 170 °C, due to the decomposition of small volatiles and free water in the sample. The peak around 400 °C represents the maximum weight loss temperature of the sample, and the CMP-containing sample exhibits the highest peak intensity and width compared with that of S0, indicating an improved residual thermal stability. The higher peak curves indicate an increase in enthalpy for the CMP samples, which also implies an improvement in the thermal stabilization of PLA by CMP.

3.4. Pyrolysis Kinetics

Pyrolysis kinetics allows for an in-depth analysis of the pyrolysis as well as the reaction mechanism. This can be used to evaluate the reaction rate and the corresponding reaction difficulty. A modified Coats–Redfern integral method was chosen to analyze the pyrolysis process for TG curves. In this approach, the reaction mechanism function G(α) is first established with reference to 29 commonly used kinetic mechanism functions. The curve of $\ln(G(\alpha)/T^2)$ versus 1/T is then plotted to calculate the apparent activation energy (E_α), based on which the thermal decomposition behavior during the TG test is systematically analyzed [39]. The calculation equations are shown in Equations (6)–(9). The image is plotted as shown in Figure 7.

$$f(\alpha) = \frac{3}{2}(1-\alpha)^{\frac{4}{3}}\left[(1-\alpha)^{-\frac{1}{3}} - 1\right]^{-1} \tag{6}$$

$$\frac{d\alpha}{dT} = \frac{A}{\beta}\exp\left(-\frac{E\alpha}{RT}\right)f(\alpha) \tag{7}$$

$$\ln\left[\frac{G(\alpha)}{T^2}\right] = \ln(\frac{AR}{\beta E\alpha}) - \frac{E_\alpha}{RT} \tag{8}$$

$$\alpha = \frac{m_0 - m_t}{m_0 - m_f} \tag{9}$$

$$G(\alpha) = \left[(1-\alpha)^{-\frac{1}{3}} - 1\right]^{-1} \tag{10}$$

In the calculation process, α denotes the weight conversion rate during the pyrolysis process. The initial mass of the sample, the mass at the moment of t, and the final mass at the end of the pyrolysis are denoted by m_0, m_t, and m_f, respectively. And t is the absolute temperature in K, A is the pre-counting factor in min^{-1}, E_α is the activation energy in kJ/mol, β is the heating rate (20 °C/min), and R is the universal gas constant (8.314 $J\cdot(mol\cdot K)^{-1}$). The experimental results indicated that a three-step chemical model was determined for the pyrolysis process, and the value of G(α) is shown in Equation (10).

Table 5 presents a detailed decomposition process for each sample, which is divided into four stages: (1) 87~296 °C, (2) 296~405 °C, (3) 405~884 °C, and (4) 884~1000 °C. Generally, a higher activation energy implies a more complex and difficult reaction process. In the initial stage, the decomposition of small molecule volatiles and water was primarily

responsible with the reduced E_α. During the second stage, the E_α value increased from 165.04 to 191.97 kJ·mol^{-1} due to the cross-linking between MPP and COS, corresponding to the enhanced thermal stability.

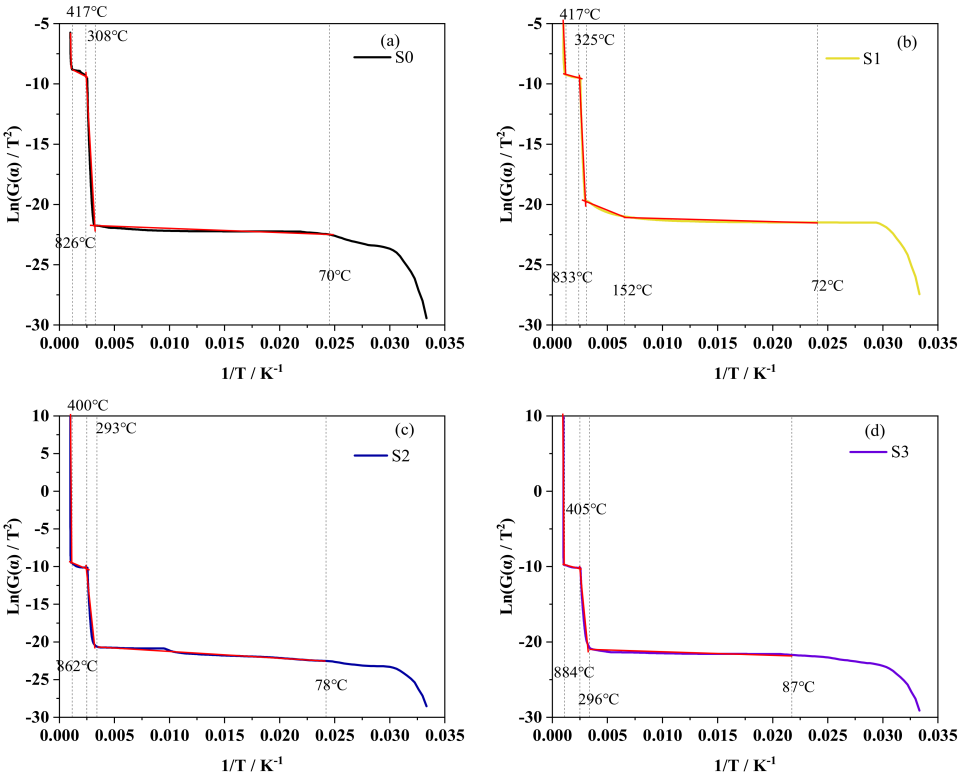


Figure 7. The fitting curve of pyrolysis kinetics. (**a**) S0; (**b**) S1; (**c**) S2; (**d**) S3. Notes: The red line in the figure is the tangent of the curve to characterize the slope.

Table 5. Pyrolysis kinetic parameters of composite PLA.

Sample	Temperature	Intercept	Slope	Adj.R^2	E_α/kJ·mol^{-1}
S0	70~308 °C	−21.77	−31	0.96	0.26
	308~416 °C	32.97	−16,242	0.98	135.04
	416~826 °C	−8.30	−387	0.99	3.22
	826~1000 °C	0.83	−8375	0.97	69.63
S1	72~325 °C	−21.01	−41.07	0.83	0.34
	325~417 °C	35.37	−16,376	0.97	136.15
	417~833 °C	−8.97	−229	0.99	1.90
	833~1000 °C	1.88	−9614	0.99	79.93
S2	78~293 °C	−20.29	−93	0.91	0.77
	293~400 °C	30.84	−20,371	0.92	169.36
	400~862 °C	−9.10	−486	0.97	4.04
	862~1000 °C	0.58	−10,098	0.93	83.95
S3	87~296 °C	−19.98	−100	0.95	0.83
	296~405 °C	39.29	−23,090	0.97	191.97
	405~884 °C	−9.34	−573	0.99	4.76
	884~1000 °C	3.86	−10,978	0.98	91.27

In the third stage, corresponding to the cleavage of hydroxyl amino groups, decomposition of MPP, and decomposition of the COS sugar ring [40,41], the E_α increased from 3.22 to 4.76 kJ·mol^{-1}. In the fourth stage, corresponding to the further decomposition of residues, the E_α value increased from 69.63 to 91.27 kJ·mol^{-1}. This indicates that the S3 exhibited higher thermal stability, which was attributed to the good adiabatic effect of the

residues. The pyrolysis kinetics quantifies the effect of CMP on the flame retardancy of PLA, and the increase in E_α verifies the improvement of the cross-linked structure on the flame retardancy.

3.5. Mechanical Properties and WCA

Figure 8 displays the stress–strain of composite PLA, as well as the hydrophobicity determined by WCA. The specific values are shown in Table 6. S0 exhibits a high tensile strength and a typical brittle fracture at 37.77 MPa. All mechanical test data and WCA in each group were obtained from five replicate experiments. The tensile strength decreased significantly after the addition of MPP, mainly due to the poor compatibility of the inorganic MPP with PLA. On the other hand, the addition of COS resulted in an improvement in tensile strength, indicating a higher compatibility between COS and PLA compared to MPP. Compared with the results of group S2, the mechanical properties of group S3 have significantly improved because the modification of bio-based COS has improved the compatibility between MPP and PLA. However, the mechanical properties are still lower than those of group S0, because COS itself contains a large number of polar functional groups such as -NH_2 and -OH, and the presence of these functional groups inevitably affects the mechanical properties of the composite PLA [42].

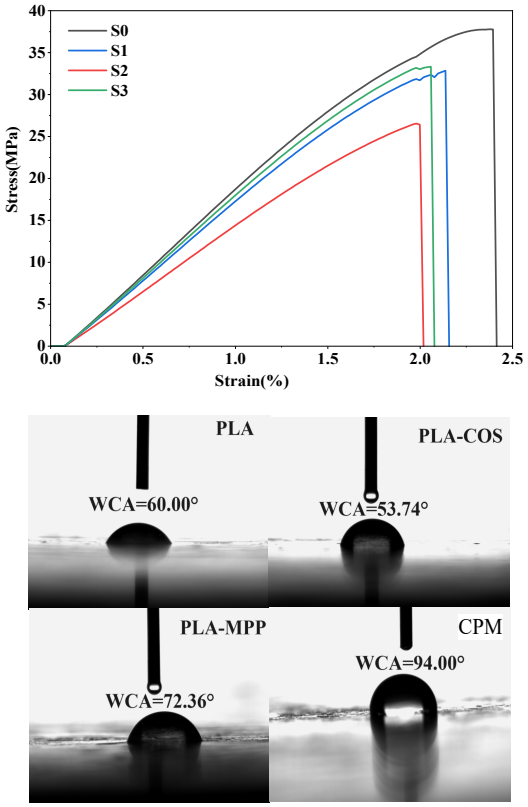


Figure 8. Stress versus strain curve of material and WCA.

Table 6. Mechanical properties of PLA composites.

Samples	Tensile Strength (MPa)	Tensile Modulus (MPa)	Elongation at Break (%)
S0	37.78 ± 2.35	1580.75 ± 96.15	2.4 ± 0.6
S1	32.84 ± 1.58	1534.58 ± 68.94	2.1 ± 0.3
S2	26.55 ± 1.91	1340.91 ± 83.46	1.9 ± 0.4
S3	33.34 ± 1.62	1630.39 ± 73.91	2.1 ± 0.3

The WCA of S2 decreased from 59.96° to 53.74° in comparison to PLA, due to the hydrophilic groups present in COS. The hydrophobicity was enhanced after doping with CMP. When MPP was incorporated, the WCA increased to 72.36°, corresponding to a rise of 34.7%. Conversely, the WCA of CMP climbed to 94.00°. Because of the hydroxylation reaction between the hydroxyl group in COS and the amino group in MPP, the hydrophilic hydroxyl group is dissociated and the hydrophobicity of PLA is improved [43]. This further improves the practical value of PLA.

3.6. Compatibility and Dispersion

As shown in Figure 9, these are the macroscopic appearances of the samples before combustion. The improved interfacial compatibility and uniform dispersion of MPP in the PLA matrix after COS modification are crucial for the superior flame-retardant efficiency. At the molecular scale, the abundant hydroxyl (-OH) and amino (-NH_2) groups on COS chains form strong hydrogen bonding and electrostatic interactions with phosphate groups on the MPP surface, enabling stable organic coating of MPP particles [44,45]. This surface modification reduces the high surface energy of inorganic MPP and suppresses its inherent agglomeration tendency. Moreover, the grafted COS segments can further form hydrogen-bond interactions with ester groups in PLA molecular chains, which effectively lowers the interfacial tension between the flame retardant and the polymer matrix, enhances interfacial affinity, and ultimately promotes homogeneous dispersion of MPP throughout the PLA matrix [46].

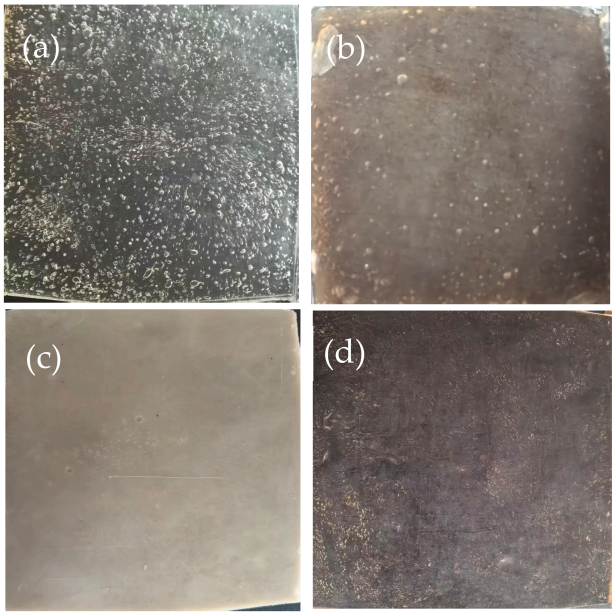


Figure 9. Appearance of (**a**) S0, (**b**) S1, (**c**) S2, (**d**) S3.

The dispersion state of flame retardants directly determines their functional efficiency in the polymer matrix. Poorly dispersed and severely agglomerated MPP forms discontinuous distribution and local defects in PLA [47,48]. During combustion, the agglomerated regions cannot form continuous and intact protective residues, leading to massive weak zones for the penetration of heat, oxygen and flammable pyrolysis products [8]. This greatly weakens the condensed-phase barrier effect and restricts the gas-phase radical scavenging effect to local areas, thus limiting the overall flame retardancy. On the contrary, uniformly dispersed CMP particles construct a homogeneous functional network in the whole matrix. Upon combustion, the C-N-P synergistic system exerts a coordinated catalytic charring and rapidly forms a dense, continuous and resilient char barrier. This barrier effectively isolates

heat transfer, oxygen diffusion and the release of combustible volatiles. Meanwhile, the gas-phase free radical quenching components act more uniformly in the combustion zone, maximizing the synergistic flame retardancy [15].

4. Discussion

CMP is fabricated through the cross-linking reaction between MPP and COS. Its flame retardancy is achieved via multiple mechanisms, including the intrinsic char formation of the bio-based carbon source within CMP, the dehydration and charring promotion of the PLA matrix by phosphoric acid sources acting as dehydrating agents, and gas-phase radical quenching and dilution. To ascertain the impact of CMP modification on PLA, FT-IR, cone calorimeter, and TG analyses were conducted. The results, summarized in Figure 10, elucidate the flame-retardant mechanism.

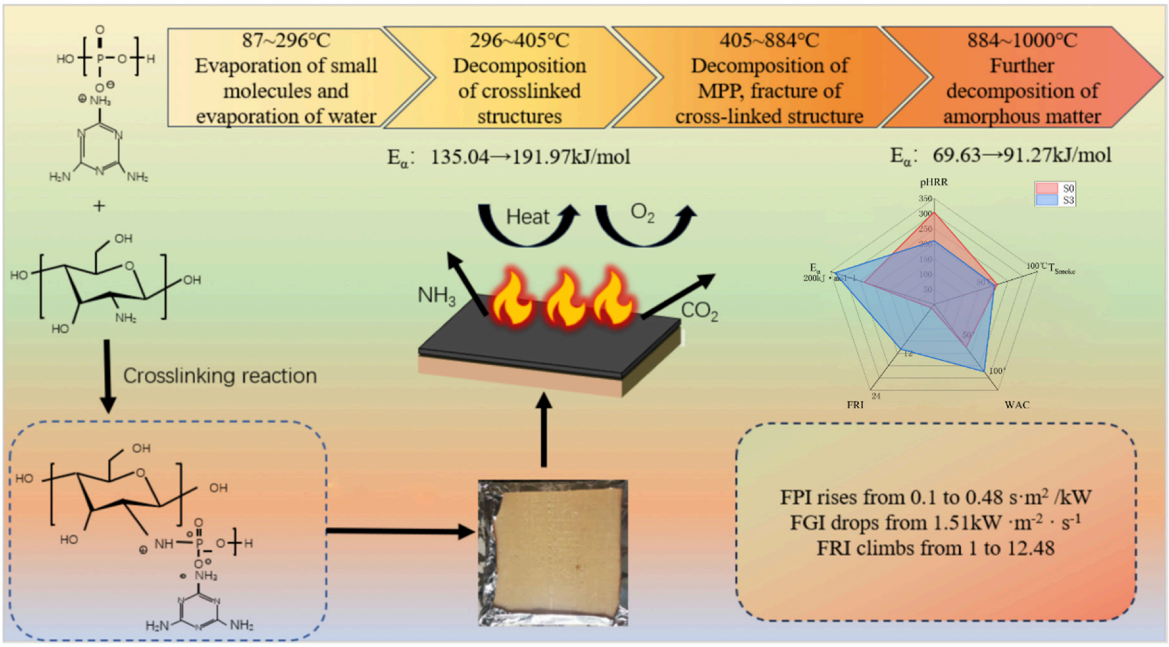


Figure 10. Mechanism of action of CMP−modified PLA.

Firstly, the doped CMP substantially enhances the PLA's flame retardancy, attributed to dual mechanisms operating in the condensed/gas phases. In the gas phase, initial pyrolysis involves the decomposition and release of intrinsic moisture within the PLA matrix, as well as water molecules generated in situ from MPP condensation [49], absorbing heat and diluting the combustible gases. Concurrently, the pyrolysis of melamine yields a self-assembled polymer network characterized by hydrogen bonding and π-π stacking interactions [50]. Furthermore, subsequent pyrolysis reactions lead to the generation and release of significant quantities of CO_2 and NH_3 [47], thereby further diluting the flammable gases and oxygen. In contrast, the combustion of PLA is a complex thermal oxidation process. Upon heating, ester bonds of PLA cleave [51], initiating a free radical chain reaction that produces flammable small molecules. The phosphorus-containing free radicals generated from MPP decomposition effectively scavenge reactive radicals such as H· and OH· [42]. This free radical scavenging effect inhibits the occurrence of chain reactions during PLA's combustion, thereby interrupting the chain reactions during combustion and improving flame retardancy. In the condensed phase, melamine undergoes self-condensation, eliminating ammonia to form a dimer. This is followed by the formation of carbonaceous structures and oligomers referred to as 'melons', which exhibit high thermal stability and remain intact even at 700 °C [52]. Simultaneously, the formation of

polyphosphoric acid promotes the charring of PLA, leading to the development of dense carbonaceous residues as a thermal barrier, insulating the underlying material from heat and preventing the influx of external O_2 [53].

Secondly, the numerous hydroxyl groups in COS form extensive hydrogen bonds with PLA, consequently leading to an elevated initial pyrolysis temperature and enhanced thermal stability [54]. This phenomenon is supported by the thermogravimetric analysis data presented in Figure 6a. However, the abundant amino and hydroxyl groups in COS can also contribute to the release of more free radicals during combustion, intensifying fire progression and resulting in a higher pHRR. Consequently, the sole addition of COS is insufficient to achieve a desirable gas-phase flame-retardant effect. As evidenced by Figure 5 and Table 2, the incorporation of CMP demonstrates a significant improvement in the condensed-phase flame retardancy of PLA. This is primarily manifested in its effective promotion of self-extinguishing behavior during fire, leading to a shortened total combustion time, reduced THR, and an increased amount of residual char after combustion. At elevated temperatures, COS undergoes ring-opening reactions and undergoes self-condensation within the PLA matrix to form aromatic structures, which effectively attenuates heat transfer [55]. Furthermore, the -NH_2 in COS decomposes to release NH_3, which further dilutes the combustible gases and oxygen. The inert gases generated during this decomposition favor the formation of stable residues, which subsequently develop an interlocking structure, thereby inhibiting the generation of flammable products [8].

Ultimately, a cross-linked network is constructed between MPP and COS, thereby achieving superior flame retardancy via the gas and condensed phase synergistic effect. During 296–405 °C, this cross-linked network begins to decompose, initiating the formation of flame-retardant residues. This process significantly increases the decomposition difficulty of the PLA substrate, as evidenced by the corresponding rise in the E_α from 135.04 to 191.97 kJ·mol^{-1}. The decomposition of COS primarily occurs at 276 °C, accompanied by processes such as sugar ring dehydration and depolymerization [56]. Between 300 and 400 °C, MPP decomposes into non-flammable gases, including polyphosphoric acid and its derivatives, melamine derivatives, and NH_3. The phosphorus-containing free radicals generated during MPP decomposition are capable of not only scavenging radicals such as H· and OH· produced by PLA pyrolysis but also those generated by COS pyrolysis. This dual radical scavenging mechanism effectively mitigates any adverse effects introduced by the addition of COS. Phosphoric acid and its derivatives catalyze the dehydration and depolymerization of sugar rings of COS, thereby accelerating char layer formation [57]. Concurrently, these acidic species also promote the dehydration and charring of the PLA substrate itself. The high-quality residues formed by COS and the substantial char layer resulting from PLA dehydration and carbonization become interlinked, which not only enhances its quality but also increases its thickness. CMP thus exerts its comprehensive C-N-P synergistic flame-retardant effect: from early-stage free radical quenching and gas-phase dilution to the condensed-phase barrier protection afforded by a high-quality char layer in the intermediate and late stages, effectively isolating the substrate from flammable gases.

Traditional phosphorus-based flame retardants are typically plagued by high required loadings and poor polymer compatibility [35]. For instance, Liu et al. enhanced the flame-retardant efficiency of intumescent flame retardants (IFR) by depositing layered double hydroxides onto MPP. Their formulation necessitated a loading of 16% to achieve peak flame retardancy, yet this compromised the mechanical integrity of polypropylene [53]. In stark contrast, our study demonstrates that a mere 7% addition of MPP, modified with the bio-based COS to improve its compatibility with PLA, achieves high-efficiency flame retardancy. Addressing the aforementioned shortcomings of phosphorus-based flame retardants, Wang et al. [58] developed a fully bio-based intumescent flame retardant through

the cross-linking of phytic acid, L-citrulline, and chitosan. While their coating exhibited enhanced flame retardancy at reduced loadings, it did not achieve the significant reduction in peak heat release rate (pHRR) observed in this study (31%). Furthermore, as evidenced by our control group S2, the char layers formed by conventional phosphorus-based flame retardants often suffer from inadequate thermal stability, leading to decomposition and failure at elevated temperatures. To overcome this, Decsxo et al. enhanced char layer quality and achieved synergistic flame retardancy by incorporating metal ions into aluminum-tris-(diethylphosphinate) [9]. This work leverages bio-based carbon sources to simultaneously bolster the thermal stability of the non-flammable residues and enhance the compatibility of MPP.

5. Conclusions

A novel flame retardant, CMP, was developed by modifying COS with MPP. The bio-based material COS was found to enhance the compatibility between MPP and PLA, exerting enhanced flame retardancy via the synergistic charring effect of MPP and COS. A range of techniques were used to assess the impact of various flame retardants on the flame retardancy. The following conclusions were drawn:

(1) The incorporation of CMP improves the flame retardancy of PLA composites. Specifically, compared to PLA, the p-HRR exhibits a reduction of approximately 31%. Furthermore, the values for the FPI and FGI were observed to shift from 0.1 $kW \cdot m^{-2} \cdot s^{-1}$ and 1.51 $s \cdot m^{-2} \cdot s^{-1}$ to 0.48 $kW \cdot m^{-2} \cdot kW^{-1}$ and 1.03 $kW \cdot m^{-2} \cdot s^{-1}$, respectively.

(2) TG analysis demonstrated that the incorporation of CMP conferred enhanced thermal stability upon PLA. Concurrently, pyrolysis kinetic analysis unveiled that the cross-linking reaction was responsible for elevating the E_α from 135.04 to 191.97 $kJ \cdot mol^{-1}$ during 296~405 °C.

(3) The hydrophobicity of the sample has been improved. The WCA of the CMP-containing sample increased from 60° to 94°; its mechanical properties are improved compared to those with MPP added.

Author Contributions: Conceptualization, M.Z., G.D. and Y.W.; methodology, X.L., M.Z. and Y.W.; software, J.G., M.Z. and Y.Z.; validation, M.Z., Y.W. and Y.Z.; formal analysis, Y.W.; investigation, M.Z., C.X., Y.L., G.D. and Y.W.; resources, M.Z., L.L., G.D. and J.G.; data curation, M.Z., G.D. and Y.W.; writing—original draft preparation, G.D. and M.Z.; writing—review and editing, Y.W. and J.G.; visualization, Y.W. and X.W.; supervision, Y.W. and X.W.; project administration, G.D. and J.G. All authors have read and agreed to the published version of the manuscript.

Funding: This research received no external funding.

Data Availability Statement: Dataset available on request from the authors.

Conflicts of Interest: The authors declare no conflicts of interest.

References

1. Khan, A.; Sapuan, S.M.; Yusuf, J.; Siddiqui, V.U.; Zainudin, E.S.; Zuhri, M.Y.M.; Tuah Baharuddin, B.T.H.; Ansari, M.A.; Rahman, A.A.A. An examination of cutting-edge developments in bamboo-PLA composite research: A comprehensive review. *Renew. Sustain. Energy Rev.* **2023**, *188*, 113832. [CrossRef]
2. Hussain, M.; Khan, S.M.; Shafiq, M.; Abbas, N. A review on PLA-based biodegradable materials for biomedical applications. *Giant* **2024**, *18*, 100261. [CrossRef]
3. Ji, Q.; Wei, J.; Yi, J.; Zhang, L.; Ma, J.; Wang, Z. Study on the static and dynamic mechanical properties and constitutive models of 3D printed PLA and PLA-Cu materials. *Mater. Today Commun.* **2024**, *39*, 108690. [CrossRef]
4. Zhong, Q.; Wang, C.; Ye, G.; Guo, Z.; Sai, T.; Hong, M.; Song, P.; Wang, H.; Huo, S.; Liu, Z. Bio-based, selenium/schiff base-containing co-curing agent enables flame-retardant, smoke-suppressive and mechanically-strong epoxy resins. *Chem. Eng. J.* **2025**, *523*, 168756. [CrossRef]

5. Zhou, W.; Liu, B.; Dai, X.-Z.; Zhou, C.; Cai, S.-X.; Sung, K.-L.P. Effect of basic amino acid on acid accumulation during poly(D, L-lactide-co-glycolide) degradation in vitro. *J. Clin. Rehabil. Tissue Eng. Res.* **2008**, *12*, 7183–7186.
6. Xia, C.; Li, C.; Lv, Y.; Wang, D.; Deng, J.; Tang, Z.; Jiang, X.; Lv, S. Recycling waste polypropylene in asphalt binders: A sustainable MPP-OMMT composite for enhanced compatibility, rheological performance, and aging resistance. *J. Clean. Prod.* **2026**, *540*, 147465. [CrossRef]
7. Zhang, Y.; Zhang, Y.; Shi, J.; Cao, M.; Wei, X.; Shi, L.; Wang, X. Experimental and numerical study on suppressing coal dust deflagration flame with $NaHCO_3$ and MPP. *Fuel* **2024**, *358*, 130152. [CrossRef]
8. Kandola, B.K.; Pornwannachai, W.; Ebdon, J.R. Flame retardance of a bio-based furan resin: Effects of added flame retardants. *Polym. Degrad. Stab.* **2024**, *220*, 110637. [CrossRef]
9. Decsov, K.E.; Győry-Slezák, E.; Gere, D.; Ronkay, F.; Marosfői, B.B.; Lenk, S.; Bocz, K. Flame retarded recycled PET foams: Comparative analysis of gas-phase and solid-phase additive performance and feasibility. *Polym. Degrad. Stab.* **2026**, *245*, 111858. [CrossRef]
10. He, J.; Sun, Z.; Chen, Y.; Xu, B.; Li, J.; Qian, L. Grafting cellulose nanocrystals with phosphazene-containing compound for simultaneously enhancing the flame retardancy and mechanical properties of polylactic acid. *Cellulose* **2022**, *29*, 6143–6160. [CrossRef]
11. Cao, B.; Zhang, Y.; Tian, Y.; Liu, J.; Zhang, J.; Cao, W.; Liu, X.; Bao, J. One-pot and green synthesis of macromolecular P–N synergistic flame retardant and its polylactic acid composites: Composition, mechanical, flame retardancy, and crystallization performance. *Polymer* **2026**, *344*, 129491. [CrossRef]
12. Zhao, X.; Chen, L.; Li, D.-F.; Fu, T.; He, L.; Wang, X.-L.; Wang, Y.-Z. Biomimetic construction peanut-leaf structure on ammonium polyphosphate surface: Improving its compatibility with poly(lactic acid) and flame-retardant efficiency simultaneously. *Chem. Eng. J.* **2021**, *412*, 128737. [CrossRef]
13. Shao, T.; Liu, J.; Gan, L.; Gong, Z.; Long, M. Yolk-shell Si@void@C composite with chito-oligosaccharide as a C–N precursor for high capacity anode in lithium-ion batteries. *J. Phys. Chem. Solids* **2021**, *152*, 109965. [CrossRef]
14. Chen, X.; Cui, X.; Sun, J.; Li, H.; Gu, X.; Zhang, S. Enhanced flame retardancy and accelerated degradation of polylactic acid using a chitosan-based additive with phosphorus and zinc. *Int. J. Biol. Macromol.* **2025**, *293*, 139184. [CrossRef] [PubMed]
15. Moussa, A.; Crépet, A.; Ladavière, C.; Trombotto, S. Reducing-end "clickable" functionalizations of chitosan oligomers for the synthesis of chitosan-based diblock copolymers. *Carbohydr. Polym.* **2019**, *219*, 387–394. [CrossRef] [PubMed]
16. Xu, P.; Luo, Y.; Zhang, P. Interfacial architecting of organic–inorganic hybrid toward mechanically reinforced, fire-resistant and smoke-suppressed polyurethane composites. *J. Colloid Interface Sci.* **2022**, *621*, 385–397. [CrossRef] [PubMed]
17. Zhang, X.; Xu, Y.-K.; Zhao, B.; Liu, Y. The preparation, properties and flame retardant mechanism of chitosan oligosaccharide bio-based flame-retardant polyester fabrics. *Prog. Org. Coat.* **2026**, *210*, 109738. [CrossRef]
18. *ISO 5660-1:2015*; Reaction-to-Fire Tests—Heat Release, Smoke Production and Mass Loss Rate—Part 1: Heat Release Rate (Cone Calorimeter Method). International Organization for Standardization: Geneva, Switzerland, 2015.
19. Shen, L.; Chi, J.; Hao, M.; Zhao, Z.; Zhang, X.; Chen, D.; Zhou, R.; Bian, H.; Jiang, J. Ant colony algorithm guided synthesis of flame retardants for enhanced polylactic acid flame retardancy. *Eur. Polym. J.* **2025**, *237*, 114192. [CrossRef]
20. Liu, B.; He, D.; Wang, Z.; Li, H.; Fang, X.; Ding, T.; Zhang, W.; Li, Z. Corrigendum to "synergistic enhancement of flame retardancy and interfacial adhesion in glass fiber-reinforced polyamide 6 composites via DOPO-functionalized maleic anhydride copolymer" [Chem. Eng. J. 522 (2025) 167686]. *Chem. Eng. J.* **2026**, *536*, 175936. [CrossRef]
21. Gong, D.; Wu, Y.; Wang, Z.; Xu, G.; Chen, X.; Jiang, Y.; Tan, L. Dual-mode intelligent polyurethane nanofibrous textile with enhanced hydrogen-bond network for thermally regulated compression and self-monitoring. *Chem. Eng. J.* **2026**, *538*, 176857. [CrossRef]
22. Tsai, H.-S.; Wang, Y.-Z. Properties of hydrophilic chitosan network membranes by introducing binary crosslink agents. *Polym. Bull.* **2008**, *60*, 103–113. [CrossRef]
23. Chen, H.; Chen, F.; Chen, H.; Liu, H.; Chen, L.; Yu, L. Thermal degradation and combustion properties of most popular synthetic biodegradable polymers. *Waste Manag. Res. J. Sustain. Circ. Econ.* **2023**, *41*, 431–441. [CrossRef] [PubMed]
24. Decsov, K.E.; Ötvös, B.; Lengyel, L.; Gere, D.; Fecske, D.; Petróczy, A.; Iván, B.; Feigl, V.; Molnár, M.; Bocz, K. Effects of phosphorus-nitrogen containing flame retardants on the compostability of poly(lactic acid). *Polym. Degrad. Stab.* **2026**, *249*, 112085. [CrossRef]
25. Feng, K.; Xin, F.; Chen, S.; Hu, J.; Chen, Y.; Gao, Z. A bio-based casein flame retardant synergist for improving phosphorus utilization efficiency: Char-forming behavior and flame retardant mechanism. *Powder Technol.* **2026**, *467*, 121553. [CrossRef]
26. Huang, Y.; Zhu, G.; Wang, Z.; Wang, Y.; Zhu, Z. The ultra-low addition of P/Si/N-containing flame retardant towards simultaneous enhancement of flame retardancy, mechanics and degradability of PLA. *Chem. Eng. J.* **2026**, *527*, 171625. [CrossRef]
27. Li, Y.; Wang, Y.; Cui, L.; Zhao, L.; Tian, Y.; Shen, J.; Zhang, J.; Xu, H.; Zhu, M. Effects of two phosphonamide flame retardants derived from biomass pyridine on flame retardancy and flame-retardant mechanism of polyamide 6. *Compos. Part A Appl. Sci. Manuf.* **2025**, *189*, 108616. [CrossRef]

28. Yang, X.; Liu, T.-S.; Hu, X.-P. Dual synergistic effect of cyano and phosphoramide-containing oligomeric flame retardant towards simultaneously improving fire safety and crystallinity of polylactic acid. *Chem. Eng. J.* **2025**, *522*, 168212. [CrossRef]
29. Das, A.; Saha, R.; Naithani, K.; Sonar, K.; Jonathan, C.; Bhowmik, S. 5′-O-P-N linkages of phosphoramidate nucleotides: Chemical construction and biological impact. *Chem. Rec.* **2025**, *25*, e202500056. [CrossRef] [PubMed]
30. Zhu, S.; Jiang, Z.; Liu, Z.; Zheng, Y.; Ge, B.; Ma, M.; Chen, S.; He, H.; Shi, Y.; Zhu, Y.; et al. Construction of environmentally friendly multifunctional core-shell flame retardant and its application in flame retardant polylactic acid. *Int. J. Biol. Macromol.* **2025**, *327*, 147497. [CrossRef] [PubMed]
31. Li, L.; Wang, G.; Guo, C. Influence of intumescent flame retardant on thermal and flame retardancy of eutectic mixed paraffin/polypropylene form-stable phase change materials. *Appl. Energy* **2016**, *162*, 428–434. [CrossRef]
32. Liu, X.; Gu, X.; Sun, J.; Zhang, S. Preparation and characterization of chitosan derivatives and their application as flame retardants in thermoplastic polyurethane. *Carbohydr. Polym.* **2017**, *167*, 356–363. [CrossRef] [PubMed]
33. Wang, M.; Zhu, Z.; Cheng, C.; Sun, H.; Li, J.; Jiao, R.; Li, A. Conjugated microporous polymer nanoparticle hollow spheres loaded with DOPO and chitosan with excellent thermal insulation and flame retardant properties. *Polym. Degrad. Stab.* **2025**, *239*, 111424. [CrossRef]
34. Iqbal, A.; Kakoria, A.; Riaz, S.T.; Xu, J.; Pushparaj, R.I.; Xu, G. Comparative fire hazards of lithium-ion battery chemistries: Linking thermal behavior, gas toxicity, and state-of-charge to composite risk profiles. *J. Power Sources* **2025**, *655*, 237914. [CrossRef]
35. Bai, Z.; Zhou, R.; Wang, Q.; Li, M.; Yan, W.; Xu, Q.; Zhou, H.; Li, X.; Yuan, R.; Guan, J.; et al. Phosphorus-functionalized schiff base flame retardant for PET and its filaments: Enhancing fire resistance, anti-dripping, and strength. *Polym. Degrad. Stab.* **2025**, *242*, 111692. [CrossRef]
36. Xu, B.; Wei, S.; Liu, Y.; Zhao, S.; Qian, L. Preparation of an organometallic complex based on phosphonitrile and its flame retardant application in epoxy resin. *J. Mater. Res. Technol.* **2022**, *21*, 4921–4939. [CrossRef]
37. Asim, M.; Paridah, M.T.; Chandrasekar, M.; Shahroze, R.M.; Jawaid, M.; Nasir, M.; Siakeng, R. Thermal stability of natural fibers and their polymer composites, Iran. *Polym. J.* **2020**, *29*, 625–648. [CrossRef]
38. Zhang, X.; Qu, X.; Guan, Q.; Li, R.; Wang, Z.; Xie, H. Rigid polyurethane foam with improved thermal stability and flame retardancy modified by barium phytate and zinc oxide. *Case Stud. Therm. Eng.* **2025**, *72*, 106261. [CrossRef]
39. Ma, Z.; Wang, J.; Yang, Y.; Zhang, Y.; Zhao, C.; Yu, Y.; Wang, S. Comparison of the thermal degradation behaviors and kinetics of palm oil waste under nitrogen and air atmosphere in TGA-FTIR with a complementary use of model-free and model-fitting approaches. *J. Anal. Appl. Pyrolysis* **2018**, *134*, 12–24. [CrossRef]
40. Affes, S.; Maalej, H.; Li, S.; Abdelhedi, R.; Nasri, R.; Nasri, M. Effect of glucose substitution by low-molecular weight chitosan-derivatives on functional, structural and antioxidant properties of maillard reaction-crosslinked chitosan-based films. *Food Chem.* **2022**, *366*, 130530. [CrossRef] [PubMed]
41. Murmu, M.; Sengupta, S.; Pal, R.; Mandal, S.; Banerjee, P. Efficient tribological properties of azomethine-functionalized chitosan as a bio-lubricant additive in paraffin oil: Experimental and theoretical analysis. *RSC Adv.* **2020**, *10*, 33401–33416. [PubMed]
42. Wang, Y.-W.; Chiang, C.-L.; Ke, C.-Y. Fabrication of novel halogen-free flame retardant containing functionalized chitosan from fisheries waste through the sol-gel technology and its fire safety performance in polyurethane resin. *Polym. Degrad. Stab.* **2025**, *231*, 111097. [CrossRef]
43. Li, P.; Ren, Y.-L.; Xu, Y.-J.; Liu, Y. One-step and multi-functional polyester/cotton fabrics with phosphorylation chitosan: Its flame retardancy, anti-bacteria, hydrophobicity, and flame-retardant mechanism. *Prog. Org. Coat.* **2025**, *203*, 109179. [CrossRef]
44. Fan, X.; Qin, A.; Liang, S.; Song, P.; Tang, Y.; Yan, C.; Xu, Y.; Liu, L. Surface electrostatic assembly for enhancing the fire safety, compatibility and mechanical performance of triazin-based intumescent flame retardant systems in styrene thermoplastic elastomers. *Polym. Degrad. Stab.* **2026**, *247*, 112000. [CrossRef]
45. Yu, B.; Wang, X.; Qian, X.; Xing, W.; Yang, H.; Ma, L.; Lin, Y.; Jiang, S.; Song, L.; Hu, Y.; et al. Functionalized graphene oxide/phosphoramide oligomer hybrids flame retardant prepared via in situ polymerization for improving the fire safety of polypropylene. *RSC Adv.* **2014**, *4*, 31782. [CrossRef]
46. Sabir, S.; Samyn, F.; Gaucher, V.; Lacrampe, M.-F.; Duquesne, S. Pioneering comparative study of two eco-friendly flame-retardant treatments on PLA/flax nonwoven and their transition to composite applications. *Polym. Degrad. Stab.* **2026**, *249*, 112086. [CrossRef]
47. Wang, M.; Yin, G.-Z.; Yang, Y.; Fu, W.; Díaz Palencia, J.L.; Zhao, J.; Wang, N.; Jiang, Y.; Wang, D.-Y. Bio-based flame retardants to polymers: A review. *Adv. Ind. Eng. Polym. Res.* **2023**, *6*, 132–155. [CrossRef]
48. Mu, X.; Jin, Z.; Chu, F.; Cai, W.; Zhu, Y.; Yu, B.; Song, L.; Hu, Y. High-performance flame-retardant polycarbonate composites: Mechanisms investigation and fire-safety evaluation systems establishment. *Compos. Part B* **2022**, *238*, 109873. [CrossRef]
49. Yan, Y.; Zhang, C.; Guo, J.; Gu, G.; Zou, G.; Yang, R. Enhancing the toughness and strength of flame-retardant PLA blends through triglycidyl isocyanurate driven reactive blending. *Chem. Eng. J.* **2025**, *519*, 165520. [CrossRef]

50. Jasinski, E.; Taguet, A.; Sonnier, R.; Otazaghine, B.; Gyppaz, F.; Auvray, T.; Ylla, N.; Bounor-Legaré, V.; Beyou, E. Influence of halloysite nanotubes onto the flame retardant performance and mechanical properties of LLDPE/EVA (70/30) polymer blends. *Polym. Test.* **2026**, *159*, 109207. [CrossRef]
51. Chen, B.; Ma, S.; Kumar, S.; Yao, Z.; Feng, W.; Zhao, J.; Zhang, X.; Cai, D.; Cao, H.; Watson, I. Pyrolysis behaviour and kinetic analysis of waste polylactic acid composite reinforced with reed straw processing residue. *Carbon Resour. Convers.* **2024**, *7*, 100226. [CrossRef]
52. Xue, Y.; Feng, J.; Ma, Z.; Liu, L.; Zhang, Y.; Dai, J.; Xu, Z.; Bourbigot, S.; Wang, H.; Song, P. Advances and challenges in eco-benign fire-retardant polylactide. *Mater. Today Phys.* **2021**, *21*, 100568. [CrossRef]
53. Liu, Z.; Hua, Y.; Liu, S.; Li, H.; Gu, X.; Sun, J.; Zhang, S. In-situ co-precipitation synthesis of Zn/Fe-LDH modified melamine polyphosphate for enhanced flame retardancy in polypropylene. *Polym. Degrad. Stab.* **2025**, *232*, 111147. [CrossRef]
54. Zhang, K.; Han, L.; Nie, Y.; Szigeti, M.L.; Ishida, H. Examining the effect of hydroxyl groups on the thermal properties of polybenzoxazines: Using molecular design and monte carlo simulation. *RSC Adv.* **2018**, *8*, 18038–18050. [CrossRef] [PubMed]
55. Li, P.; Wang, B.; Liu, Y.-Y.; Xu, Y.-J.; Jiang, Z.-M.; Dong, C.-H.; Zhang, L.; Liu, Y.; Zhu, P. Fully bio-based coating from chitosan and phytate for fire-safety and antibacterial cotton fabrics. *Carbohydr. Polym.* **2020**, *237*, 116173. [CrossRef] [PubMed]
56. Xu, H.-D.; Deng, H.-J.; Zeng, H.-M.; Yang, W.; Yao, C. Direct coupling of biobased bifunctional hydroxy-aldehyde monomers to chemically recyclable alipharomatic polyesters via dehydrogenative polycondensation. *Macromolecules* **2024**, *57*, 1546–1555. [CrossRef]
57. Ariturk, G.S.; Girisken, C.; Menceloglu, Y.Z. 4.22—Bio-based flame retardants for sustainable thermoplastic polymer applications. In *Comprehensive Polymer Science*, 2nd ed.; Sinha Ray, S., Ed.; Elsevier: Oxford, UK, 2026; pp. 714–752. [CrossRef]
58. Wang, L.; Guo, Y.; Huang, Y.; Wei, M.; Chen, Z.; Sheng, S.; Jia, H.; Jiang, P. Bio-based phytic acid–L-citrulline–chitosan flame retardant: Synthesis, flame retardancy, smoke suppression, and mechanism in transparent melamine resin coatings for oriented strand board. *Polym. Degrad. Stab.* **2026**, *243*, 111755. [CrossRef]

Disclaimer/Publisher's Note: The statements, opinions and data contained in all publications are solely those of the individual author(s) and contributor(s) and not of MDPI and/or the editor(s). MDPI and/or the editor(s) disclaim responsibility for any injury to people or property resulting from any ideas, methods, instructions or products referred to in the content.